Journal of Coastal Research	16	4	1073–1082	West Palm Beach, Florida	Fall 2000

Comparison of Wave Refraction and Diffraction Models

Jerome P.-Y. Maa†, T.-W. Hsu‡, C.H. Tsai§, and W.J. Juang*

†Virginia Institute of Marine Science
College of William and Mary
Gloucester Point, VA 23062, U.S.A.

‡Department of Hydraulics and Ocean Engineering
National Cheng Kung University
Tainan 701, Taiwan, R.O.C.

§Department of Oceanography
National Taiwan Ocean University
Keelung 202, Taiwan, R.O.C.

*Mathematic Model Division
Institute of Harbor and Marine Technology
Wu-Chi, Taiwan, R.O.C.

ABSTRACT

MAA, J.P.-Y.; HSU, T.-W.; TSAI, C.-H., and JUANG, W.J., 2000. Comparison of wave refraction and diffraction models. *Journal of Coastal Research,* 16(4), 1073–1082. West Palm Beach (Florida), ISSN 0749-0208.

Six numerical models: (1)RCPWAVE, (2)Ref/Dif-1, (3)RDE, (4)PBCG, (5)PMH, and (6)MIKE 21's EMS module, were examined for their performance on the simulation of water wave shoaling, refraction, and diffraction. Experimental data for waves traveling across an elliptic shoal were used as a standard for comparison. Although the last four models (*i.e.,* elliptic or hyperbolic model) are capable of simulating strong wave diffraction, reflection, and resonance, those capabilities were not compared because RCPWAVE, Ref/Dif-1, and the physical model experiment are only capable of simulating water wave shoaling, refraction, and weak diffraction. The Ref/Dif-1 had excellent accuracy in the prediction of wave height; the predicted wave direction, however, was not good. The RCPWAVE had accuracy problems in both wave height and direction. The next three models (RDE, PBCG, and PMH) all performed very well on the simulation of wave shoaling, refraction, and diffraction, and they practically provided the same results for the case study presented. The EMS module for Mike 21 was slightly different than the previous three. Regarding the simulation of the passing-through boundary, the PMH model was better because of the nearly exact solution for this boundary. The MIKE 21's EMS module had a faster computing pace, but no output for wave directions and was incapable of including tidal current effects were the major drawbacks.

ADDITIONAL INDEX WORDS: *Numerical models, model comparison, wave transformation, mild slope equation, elliptic equation solver.*

INTRODUCTION

Linear water wave transformation (refraction, diffraction, shoaling, reflection, and resonance) can be described using the Elliptic Mild Slope Equation (EMSE, BERKHOFF *et al.,* 1982), or the extended mild slope equation (MASSEL, 1995; CHAMBERLAIN and PORTER, 1995; PORTER and STAZIKER, 1995). Approaches in those currently available numerical models for solving the wave transformation process can be divided into four categories: (1) using a parabolic approximation to simplify the EMSE; (2) using a hyperbolic approach to replace the EMSE and seeking for the solution at the steady state; (3) using an interation method to solve the EMSE; and (4) using a direct method to solve the EMSE.

The first approach is restricted to no wave reflection and weak diffraction (RADDER, 1979). This kind of model (*e.g.,* Ref/Dif-1 from KIRBY and DALRYMPLE, 1991; RCPWAVE from EBERSOLE *et al.,* 1986) can be solved much faster. This is because of the nature of the parabolic partial differential equation and less restriction on grid size (*i.e.,* less than one fifth of the wave length) for this approach. Thus its implementation has been recommended for open coasts without structure to cause strong diffraction and reflection. Under this category, numerous studies have been conducted during the past decades (*e.g.,* KIRBY, 1986a; 1986b; 1988; DALRYMPLE *et al.,* 1989; MAA and WANG, 1995). The calculated results were mainly applied for studying longshore sediment transports and shoreline responses. The calculated wave directions from this kind of model, however, have not been extensively verified, and this is one of the objectives of this study.

Weak diffraction can be roughly defined as the change of wave direction at any place in the study domain being less than 30 degrees from the incident wave direction, which is usually selected parallel to the x axis. When the change is more than 45 degrees, it is called strong diffraction. Examples of strong diffraction can be found when waves approach the back of a breakwater or an island. In this case, a change of wave direction on the order of 90 degrees can be found. Notice that the Ref/Dif-1's capability on this issue has been improved to a maximum change of 45 degrees.

The next three categories are usually limited to small study domains. This is because the grid size requirement for solving the EMSE, or the hyperbolic equation, is small (less than $1/10$ of wave length), and thus, the computation matrix is too big to be solved economically for large study domains, *e.g.,* 50 wave lengths and more. However, if the study domain has a complicated geography and/or bathymetry, or if there is strong wave diffraction and/or reflection, and accurate results are needed, models in the next three categories are necessary because of the capability to simulate the extra phenomena: strong diffraction and reflection.

99013 received 29 July 1999; accepted in revision 19 October 1999.

Table 1. *Function capability for the selected models.*

	RDE	PBCG	MIKE 21′ EMS	PMH	Ref/Dif-1	RCPWAVE
Shoaling	Yes	Yes	Yes	Yes	Yes	Yes
Refraction	Yes	Yes	Yes	Yes	Yes	Yes
Diffraction	Yes	Yes	Yes	Yes	Weak	Weak
Reflection	Yes	Yes	Yes	Yes	No	No
Resonance	Yes	Yes	Yes	Yes	No	No
Spectral	P	P	P	P	P*	P
Bottom Friction	Yes	Yes	Yes	Yes	Yes	Yes+
Current Effect	P	P	No	P	Yes	P
Step slope and Bottom curvature	Yes	Yes	P	Yes	P	P
Passing-through B.C.	2nd	2nd	Sponge Layers	High Order	N/A	N/A

P: Although possible, this feature has not been implemented.
P*: The new version, Ref/Dif-S, deals with spectrum waves, but wave-wave interaction is still excluded.
1st: For the passing-through boundary condition, this level indicates that there will be errors caused by introducing wave reflection if the wave angle β (Figure 1) is more than 10 degrees.
2nd: This level means that there will be errors caused by introducing wave reflection if β is more than 30 degrees.
High Order: This level allows $\beta \approx 90$ degrees without introducing reflective waves.
Weak: The model will fail if the wave angle turns more than 30 degrees from the computing x direction. For the Ref/Dif-1 model, however, 45 degrees is still possible because of the treatment given by KIRBY (1986b).
Sponge layer: This layer can be used to absorb wave energy, and thus, is similar to that allowing waves to pass through.
+: The effect of bottom friction is an add-on process by MAA and KIM (1992).

In the second approach, which deals with a transient mild slope equation (COPELAND, 1985; MADSEN and LARSEN, 1987; ISOBE, 1994) and looks for the results at steady state, there are two models selected in this comparison: (1) MIKE 21's EMS module, and (2) the PMH model (HSU and WEN, in review). The differences between this category of models and other EMSE models are (1) the treatment of passing-through boundary conditions, (2) the different algorithm for solving the governing equation, (3) the difference in the governing equation, and (4) the direct inclusion of the wave breaking process in the model because of the iteration in time domain. Otherwise this approach should give the same results as those from the other EMSE models. The computing speed and accuracy, of course, depends on the criterion selected for convergence.

The next two approaches deal with the EMSE directly. For better handling of irregular harbor geometries, finite element methods (*e.g.*, BEHRENDT, 1985; CHEN and HOUSTON, 1987) have prevailed for the past decade. These kinds of models, however, are relatively difficult to maintain and upgrade, and thus, are excluded in this comparison. Because of the small grid size requirement, the finite difference methods can also be used to obtain an excellent approximation of a complex geometry. Iteration methods prevailed when using the finite difference approximation because of the reasonable computer memory requirements, *e.g.*, Multi-grid method (LI and ANASTASIOU, 1992), Conjugate Gradient method (PANCHANG *et al.*, 1991), Generalized Conjugate Gradient (GCG) method (LI, 1994a), and Preconditioned Bi-conjugate Gradient (PBCG) method (MAA *et al.*, 1998a). Although the convergent rate is usually good, it may degrade if the computation domain is not simple. Because the computing pace for models in this category is not as good as that from the model given next, only the PBCG model was selected for comparison.

The last approach, using the Gaussian elimination method (DONGARRA *et al.*, 1979) to directly solve the EMSE, was only possible recently because a special book-keeping procedure was developed to work with the Gaussian elimination method (RDE model, MAA and HWUNG, 1997; MAA *et al.*, 1998b). With this approach, the program coding is simple and straight-forward. Thus, program maintenance and upgrades are easy.

Since there are so many models available, it would be helpful if a demonstration of the strengths and weaknesses of each selected model was provided. To achieve this goal, models (RDE, PBGC, PMH, EMS module for Mike 21, Ref/Dif-1, and RCPWAVE) from each category were selected based on availability and necessity (Table 1). A brief description of each selected model was given first, and then, the performance of each model on wave shoal, refraction, and diffraction across the elliptic shoal experiment carried out by BERKHOFF *et al.* (1982) was examined.

BASIC MODEL EQUATIONS

The following governing EMSE, with the enhancement for large bottom slope, bottom curvature (MASSEL, 1995), and bottom friction, is the basic equation used in most models, except the EMS module for Mike 21.

$$\frac{\partial^2\varphi}{\partial x^2} + \frac{\partial^2\varphi}{\partial y^2} + \frac{e_0}{h}\left(\frac{\partial h}{\partial x}\frac{\partial\varphi}{\partial x} + \frac{\partial h}{\partial y}\frac{\partial\varphi}{\partial y}\right) + k^2\left(1 + \psi + \frac{if_d}{n\sigma}\right)\varphi = 0 \quad (1)$$

where

$$\psi = e_1(kh)\left[\left(\frac{\partial h}{\partial x}\right)^2 + \left(\frac{\partial h}{\partial y}\right)^2\right] + \frac{e_2(kh)}{k_o}\left(\frac{\partial^2 h}{\partial x^2} + \frac{\partial^2 h}{\partial y^2}\right) \quad (2)$$

e_0, e_1, and e_2 are three functions of relative depth (kh), φ is the velocity potential function in the study domain for a simple harmonic wave flow, $i = (-1)^{1/2}$, f_d is a friction coefficient (DALRYMPLE *et al.*, 1984), $\sigma = 2\pi/T$ is the wave frequency, $k_o = 4\pi^2/gT^2$ is the deep water wave number, T is the wave period, g is the gravitational acceleration, $n = (1 + 2kh/\sinh 2kh)/2$, $k = 2\pi/L$ is the local wave number, L is the local wave

length, h is the water depth, $\partial h/\partial x$ and $\partial h/\partial y$ are bottom slopes in the x and y directions respectively, $\partial^2 h/\partial x^2$ and $\partial^2 h/\partial y^2$ are bottom curvatures in the x and y directions, respectively, and x and y are the two horizontal coordinates.

Among the six selected models, the RDE and PBCG models followed Eq. 1 exactly. The PHM model and EMS module had an extra transit term and other means to transform the governing equation. The other two models were simplified with different degrees. Details will be given when presenting each model.

The boundary conditions can be described by the following two equations (BEHRENDT, 1985):

$$\frac{\partial \varphi}{\partial x} = i\alpha k_x \varphi + 2ik\varphi^g, \quad \text{on x direction}$$

$$= iak\varphi\sqrt{1 - \left(\frac{k_y}{k}\right)^2} + 2ik\varphi^g,$$

$$\cong \pm i\alpha k\varphi + 2ik\varphi^g, \quad \text{1st order on } \pm x \text{ direction}$$

$$\cong \pm i\alpha k\left(\varphi + \frac{1}{2k^2}\frac{\partial^2 \varphi}{\partial y^2}\right) + 2ik\varphi^g,$$

$$\text{2nd order on } \pm x \text{ boundary} \quad (3)$$

$$\frac{\partial \varphi}{\partial y} \cong \pm i\alpha k\left(\varphi + \frac{1}{2k^2}\frac{\partial^2 \varphi}{\partial x^2}\right) + 2ik\varphi^g,$$

$$\text{on } \pm y \text{ boundary} \quad (4)$$

where k_x and k_y are wave number components in the x and y directions, respectively. This condition can be used as (1) total reflection (with $\varphi^g = \alpha = 0$), (2) partial reflection, (with $\varphi^g = 0$, and $0 < \alpha < 1$), (3) total passing through (with $\varphi^g = 0$, and $\alpha = 1$), or (4) given boundary condition (with $\varphi^g =$ given, and $\alpha = 1$). Here $\alpha = (1 - R)/(1 + R)$ and R is the wave reflection coefficient and φ^g is the given wave velocity potential. Because the angle, β (and thus, k_x), for waves approaching a boundary is unknown *in prior,* k_x has to be replaced by $(k^2 - k_y^2)^{1/2}$. Thus, the original boundary condition (the second line in Eq. 3) is a nonlinear equation and its first and second order approximations are displayed in the 3rd and 4th lines of Eq. 3, respectively. Because of the similarity, only the second order approximation is given for the y direction boundary condition, *i.e.,* Eq. 4. Equation 3 is applicable to the boundary segments that are perpendicular to the x-axis, where the positive sign is for those segments that have the water grid point on their left side. Equation 4 is applicable to those boundary segments that are perpendicular to the y-axis, and the positive sign is for those segments that have the water grid point on the bottom. When using the second-order approximation for a total or partial passing-through boundary condition, reflective waves will be introduced when β is more than 30 degrees, even assigned $\alpha = 1$. Improvements by using the third-order approximation (Eq. 5) given by KIRBY (1989) are possible if needed. With that improvement, β can be increased up to 70 degrees without causing severe wave reflection when specifying $\alpha = 1$.

$$\frac{\partial \varphi}{\partial x} + \frac{b_1}{k^2}\frac{\partial^3 \varphi}{\partial x \partial^2 y} = \pm i\alpha k\left(a_0\varphi + \frac{a_1}{2k^2}\frac{\partial^2 \varphi}{\partial y^2}\right) + 2ik\varphi^g,$$

$$\text{on } \pm x \text{ boundary} \quad (5)$$

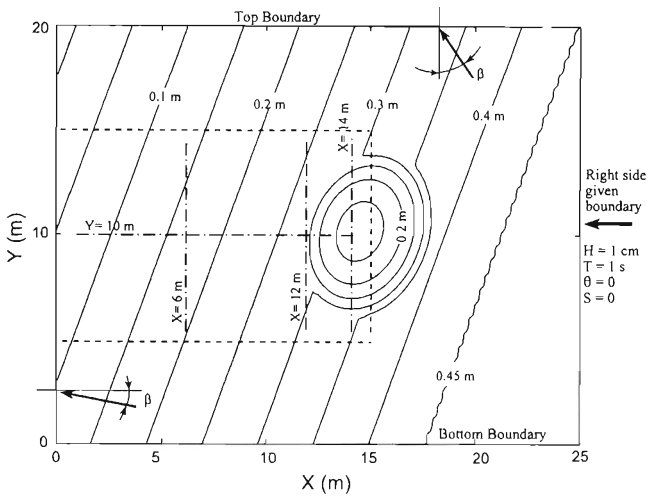

Figure 1. Bathymetry of the Elliptic Shoal. Incident wave information is given at the right boundary. Dashed box shows area with detailed wave vectors. Center lines show where the wave height profiles will be compared.

where $a_0 = 0.9945$, $a_1 = 0.8901$, and $b_1 = 0.4516$ are three constants which can be slightly tuned to find the largest range of β which gives the least wave reflection.

Although at a grid point where the given wave condition is specified, the actual velocity potential function is still unknown because of the possible scatter waves generated from the study domain. The outgoing scatter waves should pass through the boundary unaffected, and thus, $\alpha = 1$.

For a given monochromatic wave with wave height, H_g, period, T, and direction, θ (reference to the given boundary, see Figure 1), the given wave velocity potential can be calculated as (BEHRENDT, 1985)

$$\varphi^g = Ae^{iS} = \frac{igTH_g}{4\pi}e^{iS} \quad (6)$$

where A is the amplitude function and S is the phase function. For normally incident waves, the phase should be the same at all entrance grid points. For convenience and without loss of generality, we may choose $S = 0$ for this condition. For oblique incident waves, the phase function can be calculated as follows where x_L is a local one-dimensional coordinate, L is the wave length at the boundary location, and θ is the angle between the wave direction and the normal vector of the boundary.

$$S(x_L) = \frac{2\pi x_L \sin\theta}{L}, \qquad 0 \le S(x_L) \le 2\pi \quad (7)$$

The solution of Eq. 1, velocity potential function, φ, is a complex variable. The absolute value of φ can be used to find the local wave height according to Eq. 6. The local wave phase can be obtained as $S = \tan^{-1}(\varphi_i, \varphi_r)$, where the subscripts i and r represent imaginary and real parts of a complex variable, respectively. The local wave numbers, k_x and k_y can be calculated as $\partial S/\partial x$ and $\partial S/\partial y$, respectively. Finally the local wave direction can be obtained as $\theta = \tan^{-1}(k_y, k_x)$.

The above are basic for each model, the difference among these models are as follows.

RDE Model

Using the finite difference approximation, a banded matrix equation, $\mathbf{BX} = \mathbf{G}$, is established, where **B** is a banded matrix with a dimension of M × N, N is the length of the banded matrix, M is the band width of the matrix, **X** is the unknown column matrix, with length N, that stands for the wave potential function, and **G** is another column matrix that includes the given boundary conditions as well as the radiation boundary conditions. The banded matrix equation was solved by using a thrifty Gaussian elimination method (MAA *et al.*, 1997; 1998b) which replaces the huge memory requirement with a large hard disk space requirement. In this model, water depth can be small but cannot be zero because of the linear wave theory. At a small water depth, this model may give an unrealistic large wave height if the waves are either breaking or broken. A post process software was used to identify the breaking points. After the breaking point, wave heights were limited by the water depth, but their direction unchanged.

PBCG Model

Similar to the RDE model, a matrix equation, $\mathbf{AX} = \mathbf{G}$, was established in this model, where **A** is an N × N square matrix stored in the Row Index Sparse Storage (RISS) mode, *i.e.*, only non-zero items are stored to save computer memory. Others are the same as those given in the RDE model. Using the Preconditioned Bi-conjugate Gradient method given by PRESS *et al.* (1992), this equation can be solved with iteration. The Generalized Conjugate Gradient (GCG) method (LI, 1994a) is similar to the PBCG model, but uses a different pre-conditioner, and thus, might have a better convergent rate. For the PBCG model, the convergent criterion was selected as the difference between two consecutive computing results for any grid point is less than 1.0×10^{-7}. The number of iteration and computing time are given in Table 2. The estimated computing time for the GCG model, based on 2500 iterations claimed by LI (1994a), can be found in the parenthesis in Table 2.

PMH Model

The velocity potential φ can be treated as a time-dependent variable, and thus, a new time-dependent parabolic mild slope equation was developed on the basis of using the perturbation method (LI, 1994b; HSU and WEN, in review). The difference between this equation and Eq. 1 is given below.

$$\frac{1}{cc_g}\frac{\partial^2\varphi}{\partial^2 t} = \text{Eq. 1} \tag{8}$$

where c and c_g are wave phase and group velocity, respectively. Assuming that φ is a slow varying function and $\varphi = (cc_g)^{-1/2} e^{-i\sigma t} \Phi$, the hyperbolic equation (Eq. 12) was changed to a parabolic mild slope equation as follows

$$\frac{2i\sigma}{cc_g}\frac{\partial\Phi}{\partial t} + \nabla^2\Phi + k_c^2\Phi = 0 \tag{9}$$

Table 2. *Parameters used and results in the model comparison.*

Parameters	Berkhoff 1	Berkhoff 2
H (m)	0.01	0.01
T (s)	1.0	1.0
θ (deg)	0	0
h (m)	0.04–0.45	0.04–0.45
Δx, Δy (m)	0.1	0.1
Width × Length (m)	20 × 25	20 × 22
Grid No. in x & y direction	201 × 251	200 × 220
RDE		
Computing time	1056 s	946 s
Memory required	26.20 MB	25.46 MB
PBCG		
Iterations	10,103	7,922 (2,500)**
Computing time	7,015 s	4,433 s (1,400 s)***
Memory required	11.48 MB	10.72 MB
Ref/Dif-1		
Computing time	12 s (2.6 s)*	
Memory required	2.0 MB	
RCPWAVE		
Computing time	49 s (3.2 s)*	
Memory required	2.6 MB	
EMS module for Mike 21		
Iterations	96	68
Computing time	661 s	309 s
Memory required	6.87 MB	6.11 MB
PMH		
Iterations	1,200	
Computing time	1,600 s	
Memory required	2.7 MB	

The computing time is based on a Pentium 233 Personal computer with 64 MB of memory, and Windows 95 operation system.
* The numbers in parentheses are the results using their own required grid size: Δx = 0.25 m and Δy = 0.2 m.
** Number in parentheses was given by LI (1994a) for his GCG model.
*** Number in parentheses was estimations for the GCG model.

where k_c is the equivalent wave number. The definitions and other details can be found in HSU and WEN (in review). In each computation direction, i or j, Eq. 9 can be used to form a tridiagonal matrix equation, $\mathbf{CX} = \mathbf{H}$, where **C** is a 3 × N banded matrix, and N is the length of this banded matrix in either i or j directions, **X** is the unknown column matrix, and **H** is another column matrix which includes boundary conditions.

Using the Alternating Direction Implicit (ADI) scheme with iteration, the velocity potential Φ was solved. The converged criterion is selected as $E < 10^{-4}$, where E is a residual parameter. Von Neumann's stability analysis (LI, 1994b) shows that the numerical scheme selected to solve this parabolic mild slope equation is unconditionally stable.

A special treatment of the passing-through boundary condition was implemented by HSU and WEN (in review) as follows. Although wave angles at the passing-through boundaries are unknown *in prior* in the current time step, they considered these angles to be the same as angles obtained in the previous time step. With iteration, they can obtain nearly exact solutions at the boundaries which make their Parabolic Mild slope equation model with a High (PMH) order of accuracy on the passing-through boundaries.

EMS Module for Mike 21

The Danish Hydraulic Institute's EMS module for MIKE 21 is essentially the one developed by MADSEN and LARSEN (1987). This model has a transit "mild slope equation" for water surface elevation, ζ, as follows.

$$-\frac{c_g}{c}\frac{\partial^2\zeta}{\partial^2 t} + \nabla(cc_g\nabla\zeta) = 0 \tag{10}$$

This equation can be split into three first-order equations (Eq. 11), where P and Q are pseudo fluxes in the x and y directions, respectively.

$$\frac{\partial P}{\partial t} + cc_g\frac{\partial\zeta}{\partial x} = 0$$

$$\frac{\partial Q}{\partial t} + cc_g\frac{\partial\zeta}{\partial y} = 0$$

$$\frac{c_g}{c}\frac{\partial\zeta}{\partial t} + \frac{\partial P}{\partial x} + \frac{\partial Q}{\partial y} = 0 \tag{11}$$

By further assuming that P, Q, and ζ are all slow-varying functions, the harmonic term, $e^{-i\sigma t}$, can be removed from Eq. 11 for higher computing efficiency. By including a source term in Eq. 11 to introduce the incident waves, MADSEN and LARSEN generalize Eq. 11 as a wave transformation model. The solution technique of this model is similar to that for solving the momentum and continuity equations for long waves. The final steady-state solution is the solution to the original elliptic mild-slope equation. This system of equations was solved by a highly efficient double sweep method with a variable time step for the iteration toward the steady-state solution.

The computing technique used in the EMS model requires that all boundaries be totally (100%) reflective. For this reason, incident waves have to be introduced from the interior, and sponge layers must be installed on the passing-through boundary. In the sponge layers, wave energy can be totally or partially dissipated (LARSEN and DANCY, 1983). In this case study, 10 sponge layers were set up at the left boundary and five sponge layers at the right boundary because waves mainly travel in the x direction. No sponge layer was applied on the top and bottom boundaries. Wave breaking was enabled, which dissipates the wave energy on the beach.

The output of the EMS model includes: both transient and steady-state, water surface elevations, wave heights, depth-averaged particle velocities, and radiation stresses. Although the depth-averaged particle velocities, obtained from the summation of the two pseudo fluxes (P and Q), can be plotted to show the trend of wave directions, this model does not provide wave phase or direction information.

This model is different, in a fundamental sense, from other elliptic or hyperbolic models because the dependent variable in the governing equation (Eq. 10) is water surface elevation (ζ). Strictly speaking, this model did not solve the mild slope equation of velocity potential function (Eq. 1).

RCPWAVE

In order to solve Eq. 1 (without ψ, nor the bottom friction term), EBERSOLE *et al.* (1986) substituted $\varphi = Ae^{iS}$ and obtained two equations for the amplitude function, A, and the phase function, S. They added an extra restriction, $\nabla \times \nabla S = 0$, (irrotationality of wave phase gradient) to the governing equations. They used an iteration method to solve the finite difference approximations of the three equations in the y direction which should be roughly normal to the wave propagation direction. After being converged in the iterations, the computation advanced into the next x grid. Their approach is not similar to that given by the Ref/Dif-1 model. They solved the EMSE using a numerical method that is designed for a parabolic type of differential equation. Although they have not changed the original governing equation, the numerical method they selected ignores the reflected waves, and the numerical scheme only produces stable results when the wave angles are within 30 degrees from the x axis. This model produces local wave height, phase, and wave angle, θ, directly.

Ref/Dif-1

Restricted to no wave reflection, no ψ term, and only weak diffraction, KIRBY and DALRYMPLE (1991) presented the Ref/Dif-1 model, which is quite popular in the U.S. In this model, the velocity potential function is separated into two parts: one for the progressive waves and one for the reflective waves which were discarded. Because of the use of an implicit scheme to solve the simplified equation, the computation speed is excellent. Also because of the enhancements provided by DALRYMPLE *et al.* (1984), this model remains stable even when the wave propagation direction deviates to 45 degrees from the x axis. Although this model has many enhancements, *e.g.,* wave transmission across an island (DALRYMPLE *et al.,* 1984), tidal current influence on wave transformation, computation on curve-linear coordinates (KIRBY, 1988), and weak nonlinear wave transformation (KIRBY, 1986a), the accuracy of the calculated wave direction is the major concern when using this model. We will demonstrate this point next.

The RCPWAVE and Ref/Dif-1 Models require that the grid size be less than one fifth of the wave length ($\Delta x \leq L/5$, or 0.25 m for the case study). For this reason, the computing time (see Table 2) can be reduced significantly.

RESULTS

The computing results for all the models are summarized in this section. Normalized wave height contours and wave vectors are the major items compared. For similar results, only one is presented to save space.

The elliptic shoal experiment (BERKHOFF *et al.,* 1982) was selected because it was well designed for checking wave shoaling, refraction and weak diffraction. The bathymetry of the experimental and computation domain is given in Figure 1. Waves (period = 1 sec, wave height = 0.01 m, normal incident, see Figure 1) are propagating into the study domain from the right hand side. On the left hand side, there is a beach, and a portion of the left hand side boundary (0 m < y < 17 m) has to be specified as a total-passing-through boundary (*i.e.,* $\alpha = 1$). On the top and bottom boundaries, the total-reflection boundary condition (*i.e.,* $\alpha = 0$) is specified to

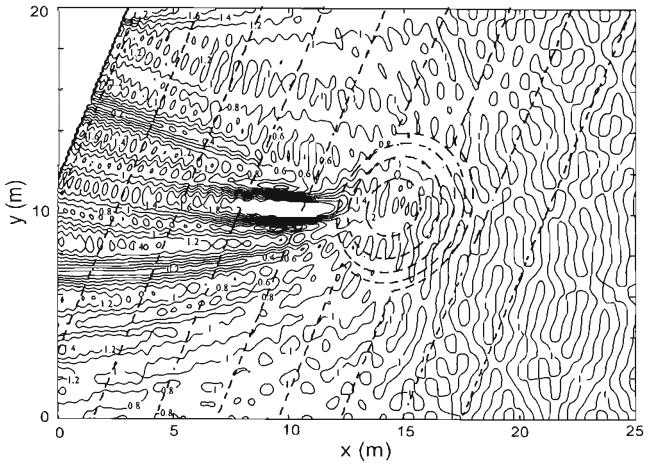

Figure 2. Calculated Wave Height Contours on the Elliptic Shoal Experiments Using the RDE, PBCG, and PMH Models. Dashed lines are bathymetric contours.

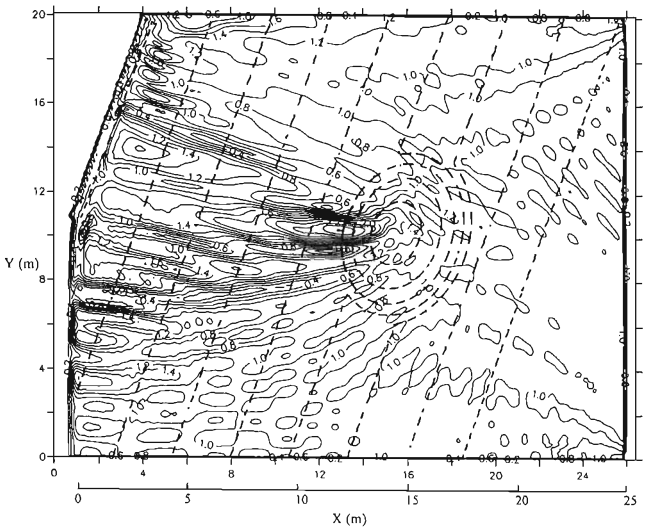

Figure 3. Calculated Wave Height Contours on the Elliptic Shoal Experiments Using the EMS module for MIKE 21. Dashed lines are bathymetric contours. The computation domain in x direction is slightly larger (26.5 m) than that from other models (25 m) because of the use of sponge layers.

simulate the wave guides used in the experiment. The grid size and other information is given in Table 2. For comparison with the GCG model (LI, 1994a), another smaller computation domain is selected and the results are given in Table 2 under the column of Berkhoff_2.

Although the experiment carried by BERKHOFF *et al.* (1982) is the best one for checking wave refraction and weak diffraction, their study cannot provide all the information needed for later studies. For example, it would be useful if they had provided a measured wave vectors plot, measured wave height contours, or measured wave crest lines. Without this information, criteria were selected as follows to justify the accuracy of the selected models: (1) The performance of each model must be checked with the available data; (2) If no experimental data for verification are available, the common results from more than one model will be selected as the background-truth. Based on the first criterion, the comparison of wave height profiles with measurements was checked. Our study, however, demonstrated that this criterion alone is not sufficient to show the accuracy of a model. Based on the second criterion, the practically-the-same wave height contour plots and wave vector plots obtained from the RDE, PBCG, and PMH models (Figures 2 and 6) were selected as the accurate results.

Because the reflective waves are negligibly small and wave diffraction is weak in the experiment conducted by BERKHOFF *et al.* (1982), the experimental results can be used to verify the performance of Ref/Dif-1 and RCPWAVE models.

Wave Height

Four normalized wave height contour plots (Figures 2 to 5), which represent the results from RDE, MIKE 21's EMS, Ref/Dif-1, and RCPWAVE models, are presented. The contours from other models (*i.e.,* PMH and PBCG) are practically the same when compared to those given by the RDE model, and thus, were omitted.

The RDE's wave height contours (Figure 2) show a slight wave reflection at the domain $x > 15$ m. These reflected waves were revealed from the normalized wave height contours oscillating around 1 at the portion before the shoal. After the shoal, wave refraction and diffraction dominate. Because the RDE model does not allow for zero water depth, a minimum water depth of 0.04 m was arbitrarily selected to establish an artificial total-passing-through boundary (see the left-top corner in Figure 2). Wave energy was allowed to pass through using the second order approximation. Because the selected 0.04 m water depth is greater than the breaking depth, the RDE model avoided the wave breaking problem. The PBCG model used the same principal, and thus, was subjected to the same limitation.

Both the PMH model and the EMS module allow zero water depth. During iterations in the time domain, these two models checked the wave breaking criterion and changed the wave height accordingly.

The EMS module for MIKE 21 also gave reasonable wave height contours (Figure 3). The predicted location of maximum wave height (at $x = 12$ m) is slightly off when compared with other model results (Figures 2 and 4 indicate this location is at $x = 10$ m). The reflected waves are not as significant as those shown in Figure 2 (results from the RDE, PBCG, and PMH models). Reflective waves can be seen only at two small areas before the shoal. Notice that this model introduces sponge layers in the computation domain (at the onshore and offshore sides), and thus, the computing domain is slightly larger than others, *i.e.*, 26.4 m $\times$ 20 m.

Because the Ref/Dif-1 and RCPWAVE models do not include wave reflection, the normalized wave height contours from these two models (Figures 4 and 5) are all exactly equal to 1 before the shoal. After the shoal, they are quite different.

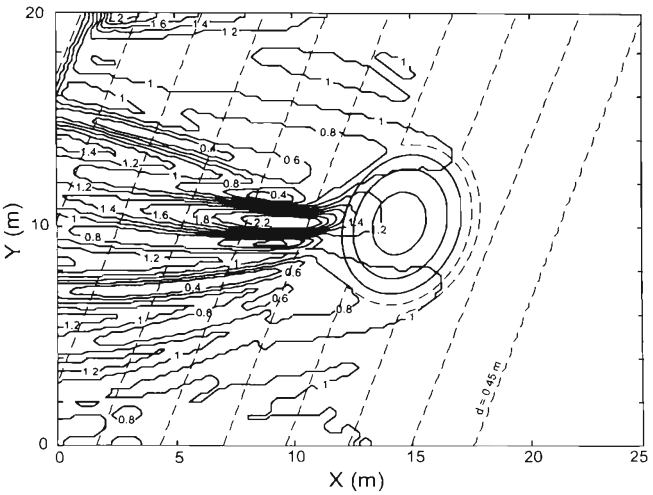

Figure 4. Calculated Wave Height Contours on the Elliptic Shoal Experiments Using the Ref/Dif-1 Model. Dashed lines are bathymetric contours.

The results from Ref/Dif-1 model (Figure 4) are very close to that given by the RDE model. Results from the RCPWAVE model (Figure 5) show large wave heights at the near coast area which were caused by the extra equation, $\nabla \times \nabla S = 0$. This extra equation can be interpreted to mean wave rays never cross each other. We will further demonstrate this point later.

Wave Vectors

A wave vectors plot shows the wave heights and directions, and thus, it is important when comparing the overall performance. For the elliptic shoal (BERKHOFF *et al.*, 1982), the

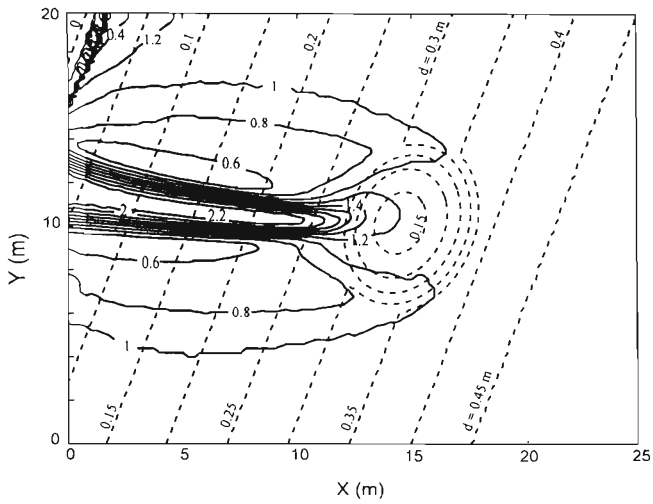

Figure 5. Calculated Wave Height Contours on the Elliptic Shoal Experiments Using the RCPWAVE Model. Dashed lines are bathymetric contours.

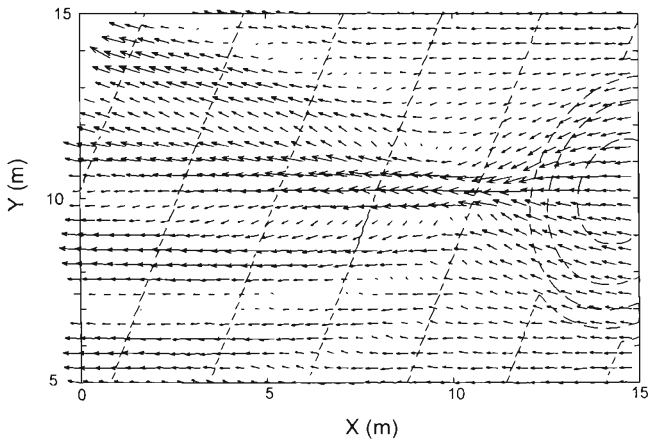

Figure 6. Calculated Wave Vectors after the Elliptic Shoal Using the RDE, PBCG, and PMH Models. Dashed lines are bathymetric contours.

change of wave vectors occurred mainly after the shoal. For this reason, only the vectors that are after the shoal were plotted (see the dashed box in Figure 1). For obtaining a clear display of the vectors, wave vector information was not plotted at every grid point. For the RDE model, wave vectors were plotted at every four grid points in both x and y directions (Figure 6). For the RCPWAVE (Figure 7) and the Ref/Dif-1 (Figure 8), wave vectors were plotted at every other grid point.

Notice that the wave vectors plot for the RDE model implies that wave trajectories may cross each other at an area behind the shoal, *i.e.*, 9 m < x < 10 m and 9 m < y < 11 m. In the wave phase contour plot (also the wave crest lines, Figure 9), this area also indicates a transition from concave wave crest lines to convex wave crest lines. This phenomenon is quite interesting and is worthy of further study.

Since the output velocity potential function represents the sum of transmitted waves, reflected waves, and diffracted

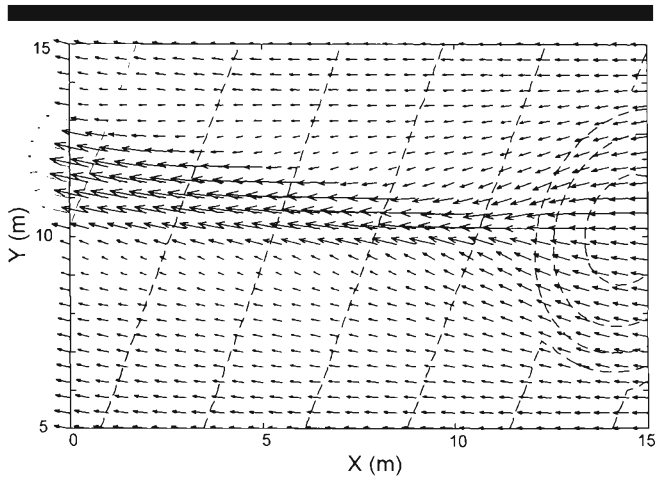

Figure 7. Calculated Wave Vectors after the Elliptic Shoal Using the RCPWAVE Model. Dashed lines are bathymetric contours.

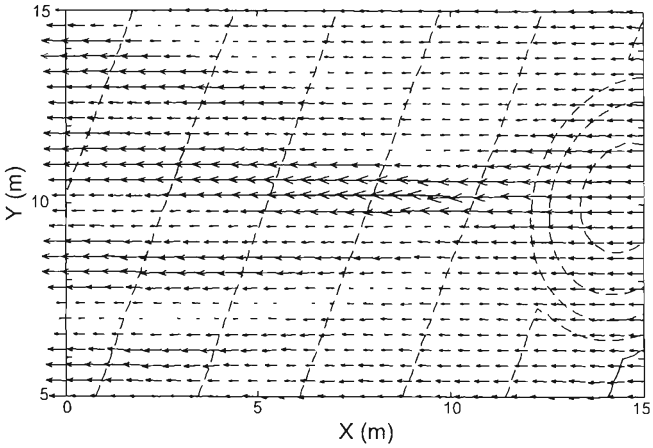

Figure 8. Calculated Wave Vectors after the Elliptic Shoal Using the Ref/Dif-1 Model. Dashed lines are bathymetric contours.

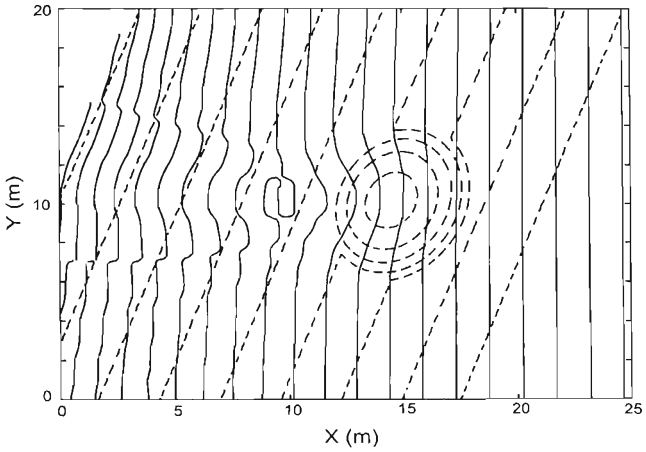

Figure 9. Calculated Wave Phase Contours (also the Wave Crest Lines) Using the RDE, PBCG, and PMH Models. Dashed lines are bathymetric contours.

waves, the wave vectors also represent the summation of these possible waves. For this reason, wave directions may change locally and are not always perpendicular to the bathymetric contours.

Notice that for $x < 8$ m in Figure 9, the wave crest lines have sharp bends located near $y = 7$ and 14 m. This kind of bending is physically unreasonable unless the wave height is small. When examining Figure 6, wave heights are very small at the above mentioned locations.

For the PBCG and the PHM models, practically identical wave vectors and wave crest lines were obtained when compared with those from the RDE model. For the MIKE 21's EMS model, wave vector information is not available for comparison.

For the RCPWAVE model, wave vectors (Figure 7) and wave height contours (Figure 5) indicate that wave height continues to increase after the shoal while traveling toward the shoreline. This phenomenon can be explained to mean the wave trajectories (Figure 10) never cross each other. The extra governing equation, $\nabla \times \nabla S = 0$, must be responsible for this result. Since the wave diffraction process allows wave rays to cross each other, the extra governing equation provided an artificial and unrealistic restriction which caused this result.

The Ref/Dif-1 model results (Figure 8) indicate that wave directions at all grid points are practically the same. It is not clear why this error occurs in the direction calculation. This unexpected finding limits the use of this model because wave direction is also important when studying longshore sediment transport.

When verifying a numerical model, previous studies only emphasized the comparison of wave heights at selected sections. We will demonstrate that this comparison alone is insufficient to judge a model's performance. In Figure 1, measurements of wave heights along the selected four center lines are available. A comparison of wave height profiles among models (RDE, RCPWAVE, Ref/Dif-1, and EMS module, see Figure 11) does not show a significant difference. This indicates that additional checks on the wave vectors or trajectories is necessary to examine the overall performance.

The predicted wave height profile from the EMS module is rougher than other models' predictions (Figure 11a). When a slightly different computing domain was selected for the EMS module, the calculated wave height profile also changed a little. This is unexpected because the computing results should be the same.

DISCUSSION AND CONCLUSIONS

For the test conditions (negligible wave reflection and weak diffraction) presented in this study, Ref/Dif-1 and RCPWAVE are the fastest models. Their predictions, however, are not always acceptable. The Ref/Dif-1 model predicts an excellent wave height distribution, but the wave direction information

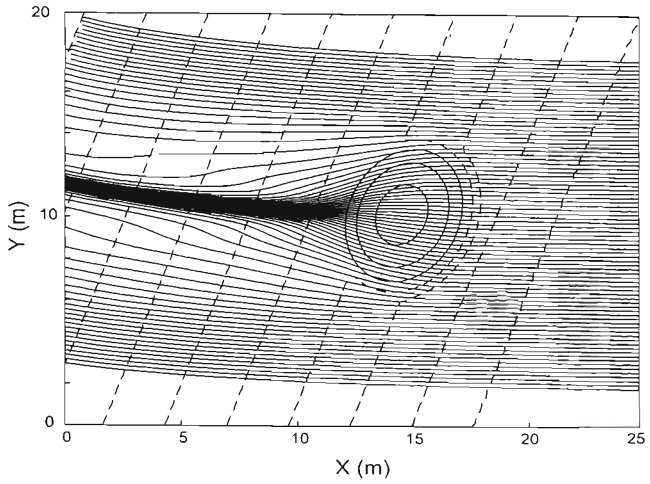

Figure 10. Calculated Wave Trajectories using the RCPWAVE model. Dashed lines are bathymetric contours.

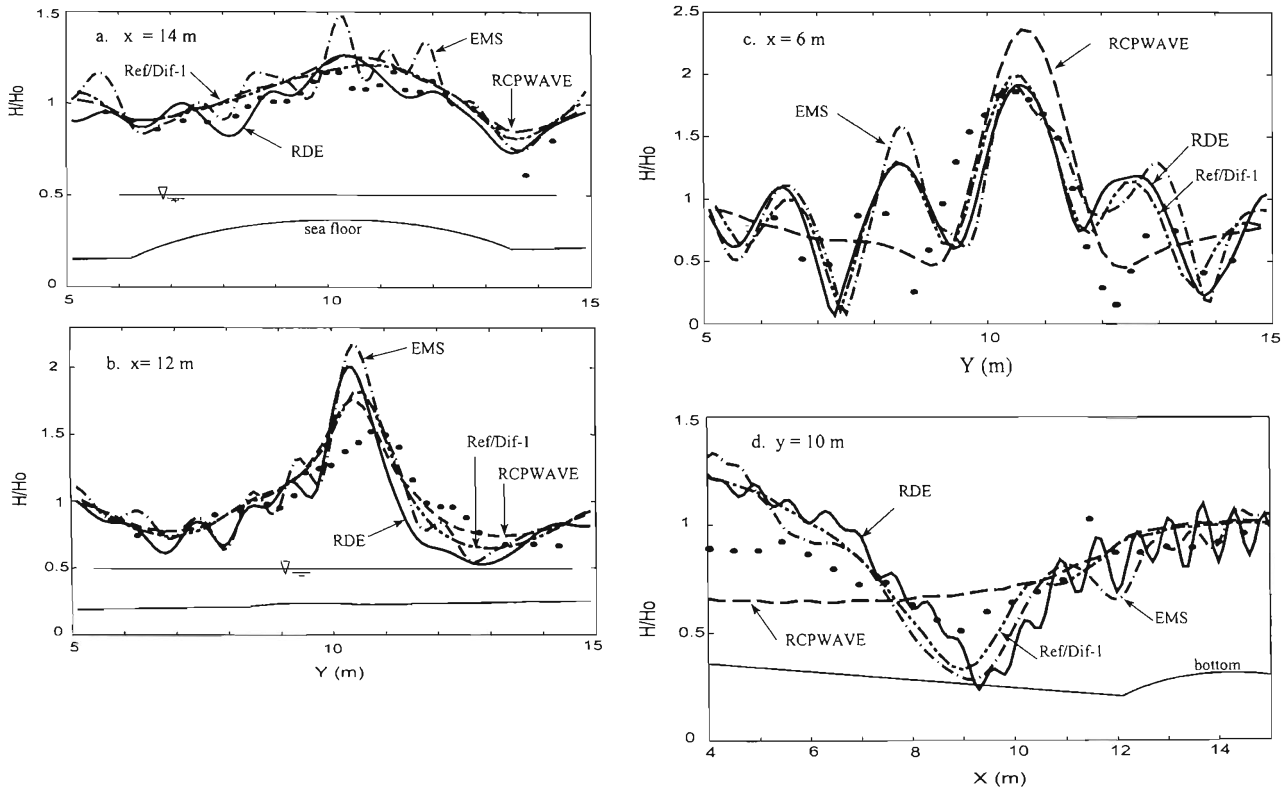

Figure 11. Comparison of Wave Height Profiles for the Selected Models. (a) at x = 14 m; (b) at x = 12 m; (c) at x = 6 m; (d) at y = 10 m. Experimental data are solid dots.

is incorrect. The RCPWAVE model cannot accurately predict the wave height distribution nor the wave direction. Thus, the use of these two models requires great caution. For any case that involves wave reflection and strong diffraction, these two models are incapable of accomplishing the job.

Among the elliptic and hyperbolic models, the RDE, PBCG, and PMH models practically produce the same wave height distribution and wave direction information. The major differences are in computer speed and memory requirements (Table 2). The above conclusion, however, is based on only one experiment where wave directions are either nearly parallel or nearly perpendicular to the boundaries. Even a first order approximation of the passing-through boundary used by the GCG model can perform well in this case. In reality, however, the wave approach angle, β (Figure 1), may easily be more than 10 degrees, and sometimes, more than 30 degrees. A higher order approximation of the passing-through boundary condition is highly recommended.

At the partially reflective boundaries, a better knowledge of the reflection coefficient is needed to specify the value of α. Laboratory experiments for a given structure can be conducted to accomplish this task. The sponge layers used in the EMS module posed a question of how to correlate the number of sponge layers to the reflection coefficient. Perhaps further numerical experiments can answer this question if the results of a physical model study on a particular type of reflective structure are already available. For a new type of reflective structure, a combination of physical and numerical experiments is necessary to address this question. For this reason, it is difficult to use this model when a new type of partially reflective structure is involved.

It is not clear why the EMS module did not provide wave direction information directly. It is impossible to interpret the wave direction information based on the output generated from the EMS module. This module, on the other hand, provides the information of wave radiation stresses. This implies that wave direction information is available internally because it is definitely needed to calculate wave radiation stresses.

Regarding other iteration methods, Li (1994a) claimed that the GCG model has a higher convergent rate (2500 iterations) for the given numerical experiment. Using the same experimental conditions, the PBCG model examined in this study required about 7700 iterations to converge. Possible reasons are (1) the GCG model has a higher convergent rate, (2) different degrees of approximation on the Newman type passing-through boundary condition, and (3) different convergent criteria. Among these three possible reasons, details for the last two are given as follows.

The GCG model used a first order approximation of the passing-through boundary condition, but the PBCG model used a second order approximation. For this reason, if $\beta >$

10 degrees, the GCG model will not give accurate results. The PBCG model, on the other hand, is good until $\beta > 30$ degrees.

The convergent criterion used in the GCG model checks the average difference of all the grid points between two consecutive calculations, but the PBCG model checks the largest difference among all the grid points between two consecutive calculations. For this reason, although they both claimed that the convergent criterion is selected as the difference less than 1×10^{-7}, the GCG model actually has a slightly easier criterion than that of the PBCG model.

Despite the differences, the computing time for the GCG model (2500 iterations, LI, 1994a) can be prorated as 1,500 s, and this is the number selected to compare with others and is listed in the parenthesis in Table 2.

It is worthwhile to mention that the experiment carried out by BERKHOFF *et al.* (1982) is not the best for checking the performance of an elliptic or a hyperbolic wave transformation model. Their experiment was well designed to prove a theoretical analysis of combining wave refraction and diffraction, but strong wave diffraction and wave reflection, however, were excluded. For verifying strong wave diffraction and wave reflection, analytical solutions and experimental data are available elsewhere (*e.g.,* GODA *et al.*, 1971; YU *et al.,* 1997). Comparison of elliptic and hyperbolic models with those available data is highly recommended, and that shall be the objective for our next study.

ACKNOWLEDGMENTS

Financial support from the U.S. Department of the Interior, Minerals Management Service, Office of International and Marine Minerals, contract number 1435-01-97-CT-30853, the National Science Council of the Republic of China, contract number NSC 86-2611-E-006-019, and the research leave of the Virginia Institute of Marine Science are sincerely acknowledged. This is contribution No. 2233 of the Virginia Institute of Marine Science.

LITERATURE CITED

BERKHOFF, J.C.W.; BOOIJ, N., and RADDER, A.C., 1982. Verification of numerical wave propagation models for simple harmonic linear water waves. *Coastal Engineering,* 6, 255–279.

BEHRENDT, L., 1985. *A Finite Element Model for Water Wave Diffraction Including Boundary Absorption and Bottom Friction.* Series Paper 37, Institute of Hydrodynamics and Hydraulic Engineering, Technical University of Denmark.

CHAMBERLAIN, P.G. and PORTER, D., 1995. The modified mild-slope equation. *Journal of Fluid Mechanics,* 291, 393–407.

CHEN, H.S. and HOUSTON, J.R., 1987. *Calculation of Water Oscillation in Coastal Harbors, HARBS and HARBD User's Manual.* Instruction Report CERC-87-2, CERC, Department of the Army, WES, Corps of Engineers, Vicksburg, Mississippi.

COPELAND, G.J.M., 1985. A practical alternative to the "mild-slope" wave equation. *Coastal Engineering,* 9, 125–149.

DALRYMPLE, R.A.; KIRBY, J.T., and HWANG, P.A., 1984. Wave diffraction due to areas of energy dissipation. *Journal of Waterway, Port, Coastal and Ocean Engineering,* 110(1), 67–79.

DALRYMPLE, R.A.; SUH, K.D.; KIRBY, J.T., and CHAE, J.W., 1989. Models for very wide-angle water waves and wave diffraction, part 2, irregular bathymetry. *Journal of Fluid Mechanics,* 201, 299–322.

DONGARRA, J.J.; BUNCH, J.R.; MOLER, C.B., and STEWART, G.W., 1979. *Linpack Users Guide.* Society for Industrial and Applied Mathematics.

EBERSOLE, B.A.; CIALONE, M.A., and PRATER, M.D., 1986. *Regional Coastal Processes Numerical Modeling System, Report 1, A Linear Wave Propagation Model for Engineering Use.* Technical Report CERC-86-4, CERC, Department of the Army, WES, Corps of Engineers, Vicksburg, Mississippi.

GODA, Y.; YOSHIMURA T., and ITO, M., 1971. *Report of the Port and Harbor Research Institute,* 10, (2).

HSU, T.W. and WEN, C.C., in review. On the radiation boundary conditions and energy dissipation for wave calculation. Submitted to *Journal of Waterway, Port, Coastal and Ocean Engineering.*

ISOBE, M., 1994. Time-dependent mild slope equations for random waves. *Proceedings of 1994 International Conference on Coastal Engineering,* ASCE, 1, 285–299.

KIRBY, J.T., 1986a. Higher-order approximations in the parabolic equation method for water waves. *Journal of Geophysical Research,* 91(C1), 933–952.

KIRBY, J.T., 1986b. Rational approximations in the parabolic equation method for water waves. *Coastal Engineering,* 10, 355–378.

KIRBY, J.T., 1988. Parabolic wave computations in non-orthogonal coordinate systems. *Journal of Waterway, Port, Coastal, and Ocean Engineering,* 114(6), 673–685.

KIRBY, J.T., 1989. A note on parabolic radiation boundary conditions for elliptic wave calculation. *Coastal Engineering,* 13, 211–218.

KIRBY, J.T. and DALRYMPLE, R.A., 1991. *User's Manual, Combined Refraction/Diffraction Model, Ref/Dif-1, Version 2.3.* Center for Applied Coastal Research, Department of Civil Engineering, University of Delaware, Newark, Delaware.

LARSEN, J. and DANCY, H., 1983. Open boundaries in short-wave simulations - A new approach. *Coastal Engineering,* 7, 285–297.

LI, B., 1994a. A generalized conjugate gradient model for the mild slope equation. *Coastal Engineering,* 23, 215–225.

LI, B., 1994b. An evolution equation for water waves. *Coastal Engineering,* 23, 227–242.

LI, B. and ANASTASIOU, K., 1992. Efficient elliptic solvers for the mild-slope equation using the multigrid technique. *Coastal Engineering,* 245–266.

MAA, J.P.-Y. and HWUNG, H.-H., 1997. A wave transformation model for harbor planning. *Proceedings, 3rd International Symposium on Ocean Wave Measurement and Analysis, WAVES 97,* i, 256–270.

MAA, J.P.-Y.; HWUNG, H.-H., and HSU, T.-W., 1998a. A simple wave transformation model, PBCG, for harbor planning. *Proceedings of the 3rd International Conference on Hydrodynamics.* Seoul, Korea: UIAM Publishers, 1, 407–412.

MAA, J.P.-Y.; HSU, T.-W., and HWUNG, H.-H., 1998b. *RDE Model: A Program for Simulating Water Wave Transformation for Harbor Planing.* Special Scientific Report No. 136, Virginia Institute of Marine Science, Gloucester Point, Virginia.

MAA, J.P.-Y.; MAA, M.-H.; LI, C., and HE, Q., 1997. *Using the Gaussian Elimination Method for Large Banded Matrix Equations.* Special Scientific Report No. 135, Virginia Institute of Marine Science, Gloucester Point, Virginia.

MAA, J.P.-Y. and WANG, D.W.-C., 1995. Wave transformation near the Virginia coast: The 1991 Halloween northeaster. *Journal of Coastal Research,* 11(4), 1258–1271.

MAA, J.P.-Y. and KIM, C.-S., 1992. The effect of bottom friction on breaking waves using the RCPWAVE model. *Journal of Waterway, Port, Coastal and Ocean Engineering,* 118(4), 387–400.

MADSEN, P.A. and LARSEN, J., 1987. An efficient finite-difference approach to the mild-slope equation. *Coastal Engineering,* 11, 329–351.

MASSEL, S.R., 1995. *Ocean Surface Waves: Their Physics and Prediction.* Singapore: World Scientific Publication.

PANCHANG, V.G.; PEARCE, B.R.; WEI, G., and CUSHMAN-ROISIN, B., 1991. Solution of the mild-slope wave equation by iteration. *Applied Ocean Research,* 13(4), 187–199.

PORTER, D. and STAZIKER, D.J., 1995. Extensions of the mild-slope equation. *Journal of Fluid Mechanics,* 300, 367–382.

PRESS, W.H.; TEUKOLSKY, S.A.; VETTERLING, W.T., and FLANNERY, B.P., 1992. *Numerical Recipes in FORTRAN: The Art of Scientific Computing.* Cambridge University Press.

RADDER, A.C., 1979. On the parabolic equation method for water wave propagation. *Journal of Fluid Mechanics,* 95(1), 159–176.

YU, Y.-X.; LIU, S.-X., and LI, Y.-S., 1997. Diffraction and refraction of multi-directional waves. *Proceedings, 3rd International Symposium on Ocean Wave Measurement and Analysis, WAVES 97,* 1, 64–77.